

Determination of natural uranium fission rate in fast spallation and fission neutron field: An experimental and Monte Carlo study

S.R. Hashemi-Nezhad^{a,*}, Igor Zhuk^b, M. Kievets^b, M.I. Krivopustov^c, A.N. Sosnin^c,
W. Westmeier^d, R. Brandt^d

^a*School of Physics, University of Sydney, A28, NSW 2006, Australia*

^b*Joint Institute of Power and Nuclear Research-Sosny NASB, 220109 Minsk, Belarus*

^c*Joint Institute for Nuclear Research, 141980 Dubna, Russian Federation*

^d*Fachbereich Chemie, Philipps University, Marburg, Germany*

Received 22 January 2008; received in revised form 26 February 2008; accepted 27 February 2008

Available online 16 March 2008

Abstract

The “Energy plus Transmutation” experimental setup of the Joint Institute for Nuclear Research (JINR), Dubna, Russia, is a lead target surrounded by a natural uranium blanket. A polyethylene plus cadmium shield is placed around the target–blanket assembly to modify the spallation and fission neutron spectra in the system. In this work the spatial distribution of natural uranium fission rate in the assembly and fission rate in the blanket were determined experimentally and compared with Monte Carlo predictions using the MCNPX 2.6C code. Besides neutron-induced fission the calculations include the reactions $^{235}\text{U}(p, f)$, $^{235}\text{U}(\pi, f)$ and $^{235}\text{U}(\gamma, f)$. Good agreements between the experimental and calculations results were obtained. The possible sources of errors in the experiment and calculations are discussed in detail.

© 2008 Elsevier B.V. All rights reserved.

PACS: 28.65.+a; 28.90.+i

Keywords: Accelerator-driven systems; Natural uranium fission; Proton-induced fission; Pion-induced fission; Photon-induced fission; MCNPX code

1. Introduction

Accelerator-driven systems (ADS) are considered to be one of the best options for cleaner, safer and economically viable methods for future nuclear energy production and nuclear waste incineration [1–3]. In these systems the spallation neutrons sustain the fission chain reaction under subcritical conditions. These spallation neutrons have an energy spectrum covering a very wide energy range of keV to GeV and are produced via interactions of high energy ions (such as protons) with extended heavy nuclide targets (such as lead see e.g. Ref. [4]).

The currently available data tables on the reaction cross-section for neutrons with energy above 20 MeV are not

complete for all elements and isotopes that can be present within an ADS [5]. Therefore, understanding the behaviour of spallation neutrons and their interaction with the nuclei present in the system has prime importance. One of the major requirements in the design of an ADS is the ability to simulate the interactions of neutrons and other secondary particles with the nuclei present in the ADS environment and to make appropriate calculations and predictions. In this work the MCNPX 2.6C code (beta version) [6] was used to simulate the interaction of the proton with target material and behaviour of the spallation neutrons and other secondary particles in the system.

The experiments reported in this paper were carried out in the Veksler and Baldin Laboratory of High Energies (VBLHE), Joint Institute for Nuclear Research (JINR), Dubna, Russia, using the NUCLOTRON accelerator of this institute.

*Corresponding author. Tel.: +61 2 93515964; fax: +61 2 93517726.

E-mail address: reza@physics.usyd.edu.au (S.R. Hashemi-Nezhad).

2. Experimental

2.1. Experimental setup

2.1.1. Energy plus Transmutation setup

The experiments were carried out using an experimental assembly in JINR known as “Energy plus Transmutation (EPT)” setup. Fig. 1a and b illustrates the schematic drawings of the EPT installation.

Detailed description of this setup is given elsewhere [7] and in the present paper only a brief explanation of its components and their arrangements is given:

- (1) The system contains four cylindrical lead targets each with diameter 8.4 cm and length 11.4 cm.
- (2) A natural uranium blanket surrounds each of the four target sections. Each uranium blanket is composed of 30 uranium rods of diameter 3.6 cm (including the Al-cladding) and length 10.4 cm hermetically sealed in aluminum cladding. The uranium rods are arranged in the form of hexagonal (triangular) lattice with pitch size of 3.6 cm. The weight of natural uranium in each blanket section is 51.6 kg and whole setup contains total of 206.4 kg of natural uranium. Each section of target–blanket is safely fixed within a steel right angle hexagonal prism container. The four target–blanket sections aligned, along the Z-axis (the target axis) with 0.8 cm gap between the sections. These gaps are used to place activation foils, track detectors and other sensors used in the study of the neutron field within the system.
- (3) The whole target–blanket system was placed within a wooden container filled with granulated polyethylene

of average density 0.7 g cm^{-3} with dimensions and the arrangements as shown in Fig. 1.

- (4) The inner walls of the container were covered with a Cd foil of thickness 1 mm.
- (5) The whole setup is mounted on a platform that can be moved on a rail and its position on the platform can be adjusted with the help of appropriate screw devices.

2.1.2. Fission sensor sample

In order to study and determine the fission rate in the EPT setup, metallic foils of natural uranium (fission-foils) were used as fissionable material (the same material as the blanket). These foils (diameter of 7 mm and thickness $\sim 0.1 \text{ mm}$) were manufactured by cold rolling and vacuum annealing of the material. As the thickness of these foils was greater than the mean range of the fission fragments in uranium ($5.41 \mu\text{m}$), the fission-foils are considered to be “thick foils”. The fission-foils were placed in close contact between two fluorophlogopite (artificial mica) track detector sheets as shown in Fig. 2a.

The fission-foil mica sandwiches were mounted on plastic sheets (sample plates) of thickness $\sim 0.2 \text{ mm}$, along the +Y-axis at different radial distances R (0, 3, 6, 8.5, 11 and 13.5 cm), as shown in Fig. 2b. Five plates each containing six samples were placed in front, back and in the three gaps between the target–blanket sections (Fig. 2c).

2.2. Proton irradiation

The setup was irradiated by a proton beam of energy 1.5 GeV in direction parallel to the target axis (shown in

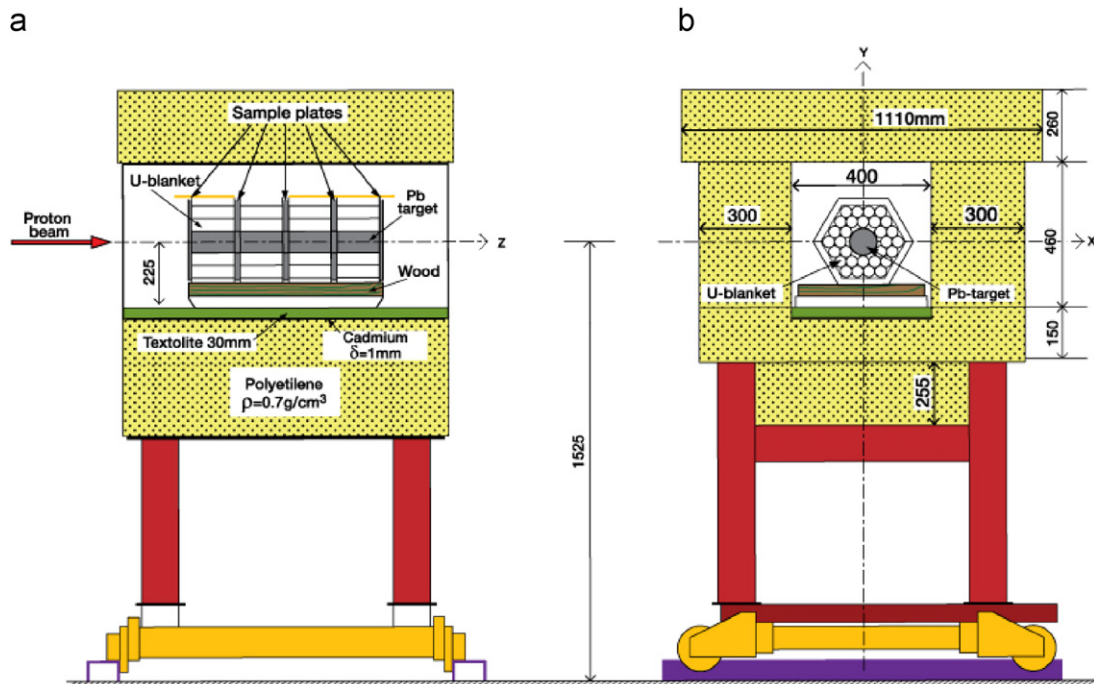


Fig. 1. Schematic drawings of the “Energy plus Transmutation” experimental setup: (a) YZ cross-section and (b) XY cross-section.

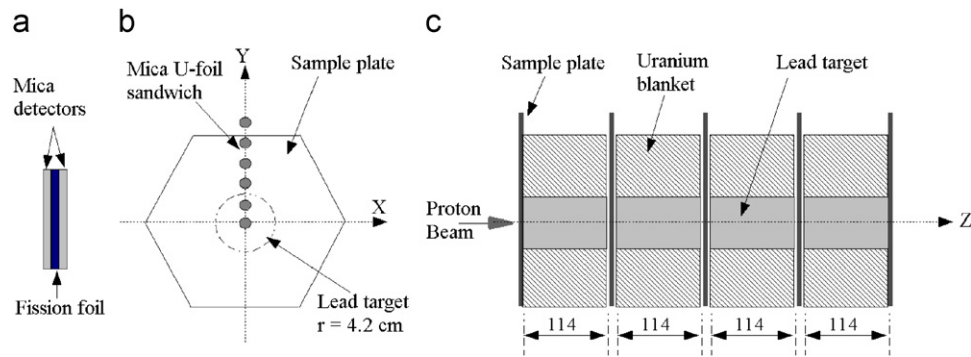


Fig. 2. (a) The schematic drawing of the fission-foil-track-detector assembly used in the experiments. (b) Schematic drawings of the sample plates and ^{235}U -mica detector sandwiches used in the experiment. (c) Placement of the sample plate within EPT assembly. Each target section is 114 mm long and there is a gap of 8 mm between each pair of target–blanket sections.

Figs. 1a and 2c). The alignment of the beam centre with the centre of the lead target was achieved by examining Polaroid films placed in front of the target and exposed to a couple proton pulses. This type of beam alignment can have an error of a few mm in X - and Y -directions.

Total fluence of the protons striking the target during the main irradiation was determined by activation of an Al-foil via the $^{27}\text{Al}(p, 3p_n)^{24}\text{Na}$ reaction [8,9]. The number of the $^{27}\text{Al}(p, 3p_n)^{24}\text{Na}$ reactions was determined by Gamma-ray spectrum analysis of ^{24}Na decay using the properly calibrated HPGe detector. The total number of protons on the system was $(1.17 \pm 0.06) \times 10^{13}$ of which $(1.12 \pm 0.05) \times 10^{13}$, i.e. 95.8% was on the target [7].

The proton beam intensity distribution along the X - and Y -axes was determined using the reaction $^{208}\text{Pb}(p, f)$ in conjunction with mica track detectors. Sandwiches of natural lead (^{208}Pb) foils of dimensions $0.7 \times 0.7 \times 0.03$ cm, in contact with mica detectors (similar to the ^{235}U -mica sandwiches; Fig. 2a) were placed on the plate 1 in front of the lead–uranium blanket setup in contact with the target (Fig. 2c) along the X - and Y -axes, extending from -13.5 to 13.5 cm both directions. Total number of these samples was 37. The incident protons ($E_p = 1.5$ GeV) induce fission in ^{208}Pb and their tracks register in the mica detectors. After exposure the track detectors were etched and track density in each sample was determined (details of the etching and counting procedures will be given in this section). The variations of the track density with distance along the X - and Y -axes were used to obtain the beam intensity distribution.

Fig. 3 illustrates the observed beam intensity distributions along the X - and Y - directions. In each of the X - and Y -directions the data were fitted with a Gaussian function and the coordinates of the beam centre (X_c and Y_c) on the target and full width at half maximum (FWHM) of the distributions were obtained from the Gaussian fits as $X_c = -0.32 \pm 0.03$ cm, $(\text{FWHM})_X = 2.01 \pm 0.06$ cm and $Y_c = -0.14 \pm 0.08$ cm $(\text{FWHM})_Y = 3.10 \pm 0.19$ cm for the X - and Y -axes, respectively.

The secondary neutrons produced in the system can also induce fission in the lead-foils. Contribution of the

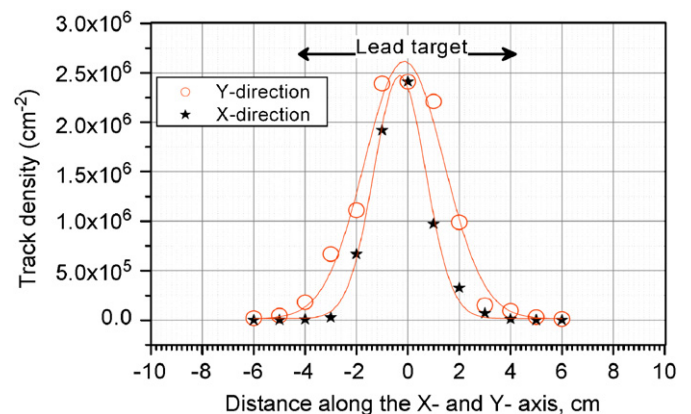


Fig. 3. The beam profile obtained using $^{208}\text{Pb}(p, f)$ reaction and mica track detector (see the text for details).

secondary neutron-induced fission, $^{208}\text{Pb}(n, f)$, to the observed fission events in the mica detectors was negligible compared to that of the $^{208}\text{Pb}(p, f)$ events produced by the primary protons. Examination of the neutron energy distribution at the centre of the plate ($X = 0$, $Y = 0$) and at position of the last lead–mica sample along the $+Y$ -direction ($X = 0$, $Y = 13.5$ cm) showed that the contribution of the secondary neutrons with energy greater than 30 MeV (energy range at which $^{208}\text{Pb}(n, f)$ cross-section becomes significant [10]) to these spectra is 8.8% and 2.1% at $Y = 0$ and 13.5 cm, respectively.

2.3. Processing of the mica detectors

After exposure the mica detectors were etched in 7% HF at 60°C . The duration of the etching time was decided on the basis of the track population in a given sample. Shorter etching times were used for samples with higher track densities, to minimize the overlapping of the track openings. To obtain an accurate measure of the track densities the tedious method of manual track counting was chosen. We counted tracks in many photomicrographs produced for each mica detector using an optical microscope. Again the overall magnification of the images was decided on the

basis of the track population in a given sample. For each foil, the mean of track density (track/cm²) in two mica detectors on its each side was determined. The accuracy of the track counting was dependent on the track population in a given mica detector.

3. Monte Carlo calculations

3.1. Calculation procedure

We used MCNPX 2.6C (beta version) Monte Carlo (MC) code [6] to simulate the behaviour of protons, neutrons and other secondary particles in our experimental setup. The experimental setup was built into the code with the characteristics given in Fig. 1 and included the natural uranium fission-foils as shown in Fig. 2.

The setup was “irradiated” with a proton beam of energy 1.5 GeV parallel to the target axis and with the beam profile and beam centre coordinates as described in Section 2.2. It was assumed that the projected beam profile on *X*- and *Y*-axes is the same as that shown in Fig. 3. The beam acceptance radius (a cylindrical tube in which the proton beam was enclosed) was set to 6 cm to include all protons including those that may hit the system beyond the target. In this case some of the protons (for probabilities, see Fig. 3) may hit the uranium blanket (and thus result in higher neutron multiplicity than in the lead) and some protons may strike the voids between the uranium rods and target (and result in no secondary particle production).

In the simulations each sample plate contained 23 or 31 fission-foils along the *Y*-axis from $Y = -13.5$ to 13.5 cm. In order to avoid confusion the fission-foils used in the MC calculations will be referred to as MC-fission-foils and will be abbreviated to MC-FF. Fig. 4 shows the experimental setup and sample plates as *seen* by the MC-code.

The following MCNPX options were used in the calculations:

1. Neutrons, protons, pions and photons were transported together with other particles allowed by the code and which could be produced by the incident protons. In these series of calculations we did not transport electrons as this slows down the calculation dramatically without causing any improvement in the calculated values.
2. Bertini intranuclear cascade (INC) model [11,12] along with RAL fission-evaporation model [13] was used. The other available models will be considered in other parts of this paper.
3. In the case of the photons, analog photonuclear particle production was used.
4. For neutrons and protons the “mix and match” option of the code was used. This option allows using the available data tables up to their upper energy limits. Then at higher energies model calculated cross-section values are used.

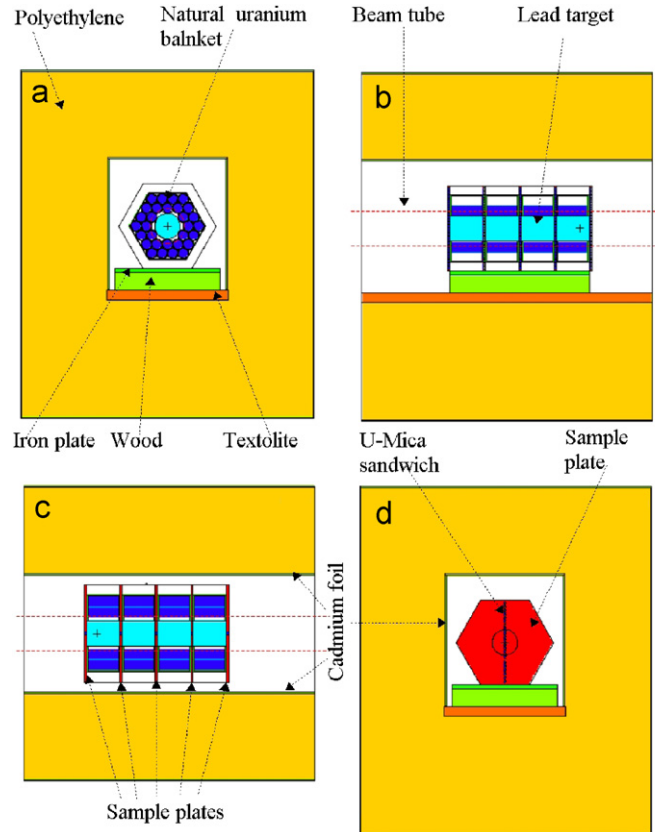


Fig. 4. The “Energy plus Transmutation” setup as seen by MCNPX 2.6C code: (a) XY cross-section; (b) YZ cross-section; (c) XZ cross-section; (d) XY cross-section through a sample plate and MC-fission-foils (MC-FF). The 31 MC-FFs were placed along the *Y*-axis. In (d) the large circle at the centre represents the XY cross-section of the hypothetical cylindrical tube of radius 6 cm, in which the proton beam is enclosed.

5. We used forced collisions in the MC-FFs to improve the statistics of the calculations.
6. High energy data tables for neutrons and protons were used whenever available [5]. Otherwise data tables of the ENDF/B-VI libraries were used.
7. In all calculations the statistical errors were less than 3% except for the case of the proton- and pion-induced fission events at large radial distances where fluxes of these particles were very low and the calculations statistics were about 6%.

3.2. Neutron spectra

Fig. 5 illustrates typical calculated neutron spectra at two radial distances ($R = 0$ and 13.5 cm) on plate 2 ($Z = 11.8$ cm). Fig. 5a shows the neutron spectra for the case when in the experimental setup both the polyethylene and Cd shields around the target–uranium assembly are present (as with the experimental setup) and Fig. 5b shows a hypothetical case when both polyethylene and Cd shields are removed.

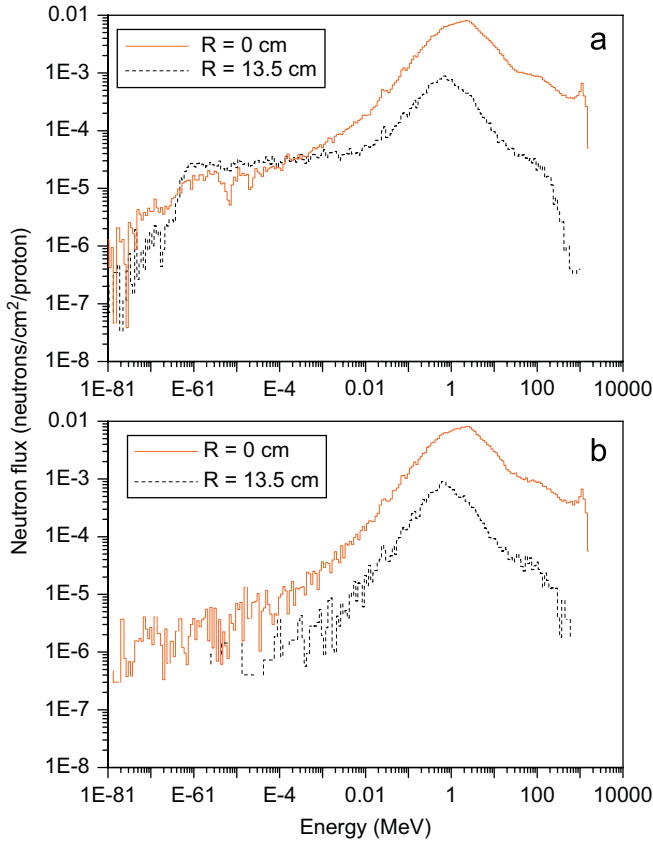


Fig. 5. Neutron energy spectra on plate 2 ($Z = 11.8$ cm) as calculated using MCNPX 2.6C code: (a) total system, containing the polyethylene and Cd shielding around the target blanket assembly and (b) hypothetical case when all material around the target–blanket assembly is removed. Equal logarithmic energy binning with 20 intervals per decade is used.

From Fig. 5 it can be seen that the presence of Cd stops thermal neutrons from entering the blanket area and the combined presence of the polyethylene and Cd shields enhances the number of the neutrons relevant to resonance absorption. This simple arrangement allows us to study (a) the interaction of the neutrons with different materials in fast and resonance spectrum within the blanket area, and (b) in thermal, resonance and fast neutron spectrum within the polyethylene section of the setup. From Fig. 5a it becomes clear that neutron spectrum becomes softer with increasing R .

4. Results and discussions

4.1. Neutron-induced fission

The track density ρ in units of (tracks cm^{-2}) is related to fission rate R_f , via following equation:

$$\rho = wR_f \quad (1)$$

where w is a calibration factor in units of $\text{tracks cm}^{-2} \text{neutron}^{-1}$ [14]. R_f is fission per atom of the fissionable nuclei in the foil induced by different particles,

during the irradiation time t and is given by

$$R_f = \sum_{i=1}^4 (R_f)_i \quad (2)$$

where $(R_f)_i$ refers to the fission rate (fission/atom, during the irradiation time t) induced by particle i (which in our case are neutron, proton, pion and photon). $(R_f)_i$ is given by

$$(R_f)_i = t \int_0^{\infty} \varphi_i(E) \sigma_i(E) dE \quad (3)$$

where $\varphi_i(E)$ and $\sigma_i(E)$ are the energy-dependent particle flux and fission cross-section, respectively. In Eq. (2), $F_i(E) = t\varphi_i(E)$ is the energy-dependent particle fluence integrated over the irradiation time t . In this paper $F_i(E)$ will be represented as follows

$$F_i(E) = N_p \phi_i(E) \quad (4)$$

where $\phi_i(E)$ is the energy-dependent particle flux per incident primary proton on the target and N_p is the total number of primary protons in the course of the target irradiation.

Neutrons that induce fission in the fission-foils have wide range of energies (Fig. 5) and angles of incidence with respect to the normal to the surface of the fission-foils [15].

It is shown that [14] the calibration factor w obtained using a specific standard neutron field can be applied to an arbitrary neutron field if in the determination of w and its subsequent use the mean track density in the track detectors on both sides of a fission-foil is used.

Using $w = (9.90 \pm 0.3) \times 10^{18} \text{ track cm}^{-2} \text{neutron}^{-1}$ for thick natural uranium fission-foil and for artificial mica detector [14] and Eq. (1), the mean track densities were converted to fission rates. It should be noted that w relates the track density in the external detector (mica) to the number of fission events within the fission-foil, regardless of the type of fission inducing particle. Also it should be noted that in the experimental determination and MC calculation of w it was assumed that all fission events are binary and the number of multiprong fission events is negligible [14].

In calculating the neutron-induced fission rates in the MC-FFs we used the following cross-section data:

1. At neutron energies $E_n \leq 20$ MeV the MCNP dosimetry data libraries (see Ref. [16]) were used.
2. At $20 < E_n \leq 257$ MeV the fission cross-section values given by Lisowski et al. [17,18] were used.
3. At energies $E_n > 257$ MeV the fission cross-sections were calculated using the XSEX3 code from the LCS-code system [19] which comes with the MCNPX 2.6C code package. The calculated cross-sections were normalized to the cross-section value of Lisowski et al. [17,18] at 257 MeV.

Fig. 6 shows the $^{238}\text{U}(n, f)$ cross-section as a function of neutron energy as obtained using the above procedure.

Fig. 7 illustrates the experimental and calculated neutron-induced fission rates as a function of the radial distance R , from the target axis (Z -axis in Fig. 2). As it can be seen the agreement between the experiment and calculation is not satisfactory, particularly at radial

distances corresponding to the target region, i.e. $R \leq 4.2$ cm.

4.2. Proton-, pion-, muon- and photon-induced fission

4.2.1. Proton-, pion- and muon-induced fission

Fission in the uranium samples and in the blanket as a whole is not only induced by secondary neutrons, but also by primary particles (protons) as well as other secondary hadrons and photons. The fission induced by particles other than neutrons can be partially responsible for the observed differences between the experimental and calculated results. Among the secondary hadrons only neutrons protons and pions are produced in significant numbers.

In these calculations possible fission events that could be induced by muons [20] have been ignored. This is for following two reasons. Firstly a very small number of muons are produced by the primary proton interactions (0.21 muons/proton). Secondly cross-section data tables for muon-induced fission are not available.

In order to estimate the contribution of proton- and pion-induced fissions to the observed track densities, proton and pion fluxes in the MC-FFs were calculated [15].

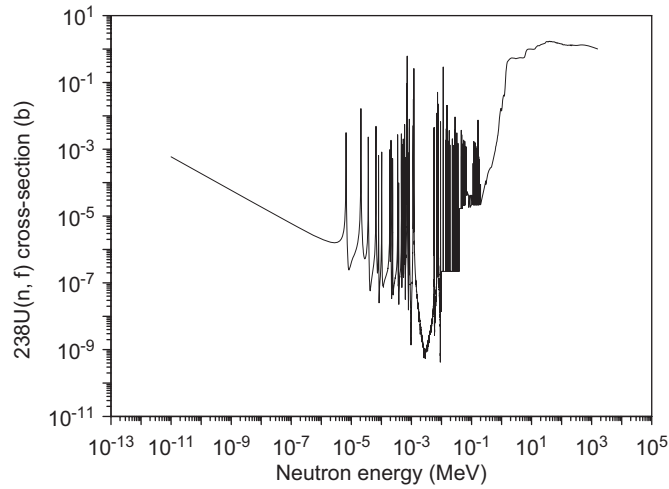


Fig. 6. $^{238}\text{U}(n, f)$ cross-section as a function of neutron energy (see the text for details).

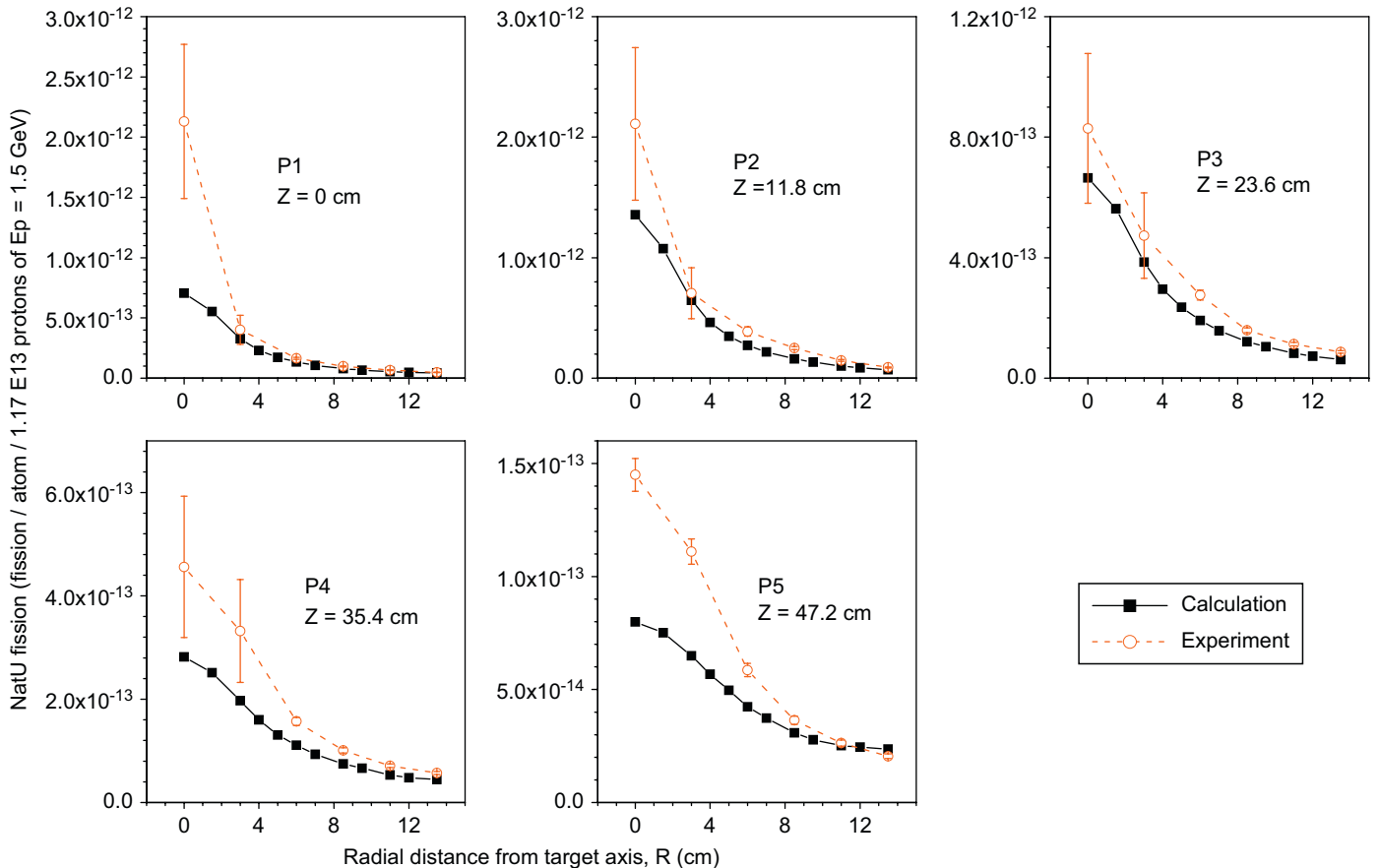


Fig. 7. Variations of ^{238}U fission rate as a function of radial distance measured from the target axis. The results for five plates at different axial distances, Z are shown. The calculations are only for neutron-induced fission. Note that the vertical scale ranges are not the same for all plots. Lines connecting the data points are drawn to guide the eyes.

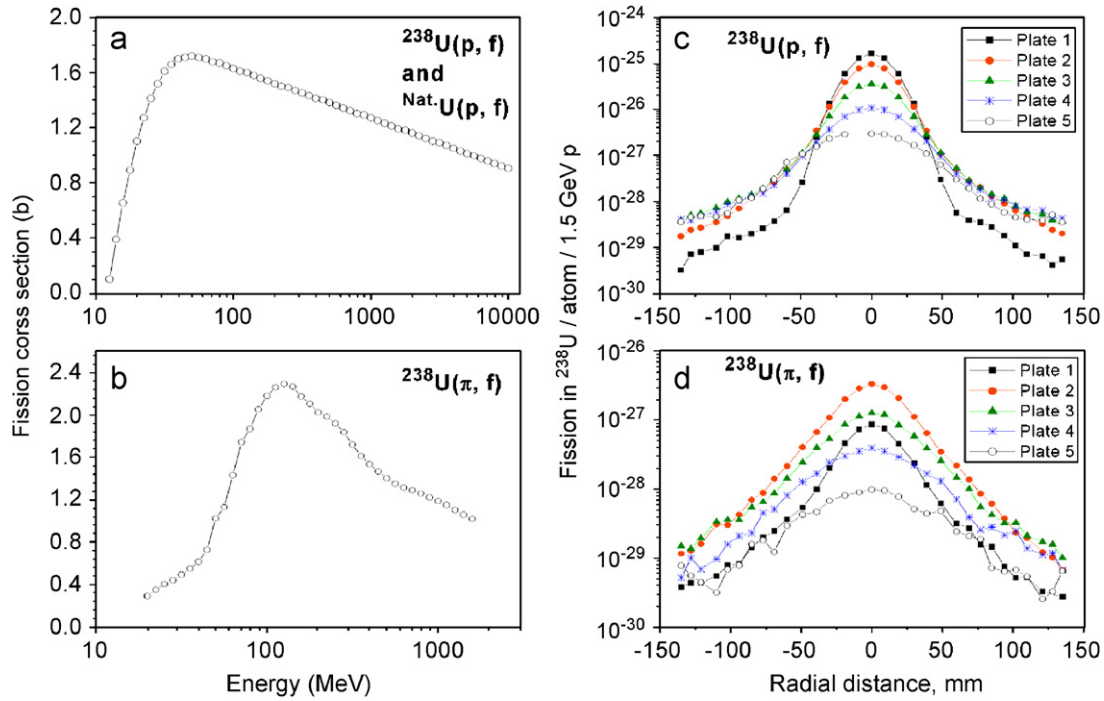


Fig. 8. (a and b) Cross-sections for $^{238}\text{U}(p, f)$ and $^{238}\text{U}(\pi, f)$ reactions (see the text for details). (c and d) $^{238}\text{U}(p, f)$ and $^{238}\text{U}(\pi, f)$ reactions rates in the EPT setup as a function of the radial distance from the target axis for five plates at different axial distance Z . The fission rates are expressed in units of “fission/atom/(1.5 GeV p)”. Lines connecting the data points are drawn to guide the eyes.

The fission cross-section, for $^{238}\text{U}(p, f)$ was calculated using the best fit curve to the available experimental data as described by Prokofiev [21]. The $^{238}\text{U}(\pi, f)$ cross-section at different pion energies were calculated using XSEX3 code and normalized to the experimentally determined $^{238}\text{U}(\pi, f)$ cross-section at pion energy of 80 MeV [22]. Fig. 8a and b show the variation of the proton- and pion-induced fission cross-sections of ^{238}U with the particle energy. In this paper we will assume that the (π, f) cross-section for ^{238}U and Nat-U is the same.

Fig. 8c and d show the calculated $^{238}\text{U}(p, f)$ and $^{238}\text{U}(\pi, f)$ fission rates (fission/atom/primary proton) as a function of the radial distance for all 31 MC-FFs in each plate and for the five plates at different Z coordinates.

XSEX3 code allows the cross-section calculation at energies above 20 MeV. It is shown that the capture of pions near nuclear surface results in a deposition of approximately 80 MeV of excitation energy in the nucleus [20]. Absorption of slow pions by ^{238}U nuclei and the subsequent fission process is predominantly a symmetric division of the nucleus (see Ref. [20] and references therein). Therefore, it is expected that slow and stopping pions would induce fission in the fission-foils and in the blanket as a whole. Consequently limiting the pion-induced fissions to energies above 20 MeV (as done in this work) will under estimate the number of such events.

4.2.2. Photon-induced fission

Fig. 9 shows the energy distribution of the photons in the blanket as calculated using the MCNPX 2.6C code. As can

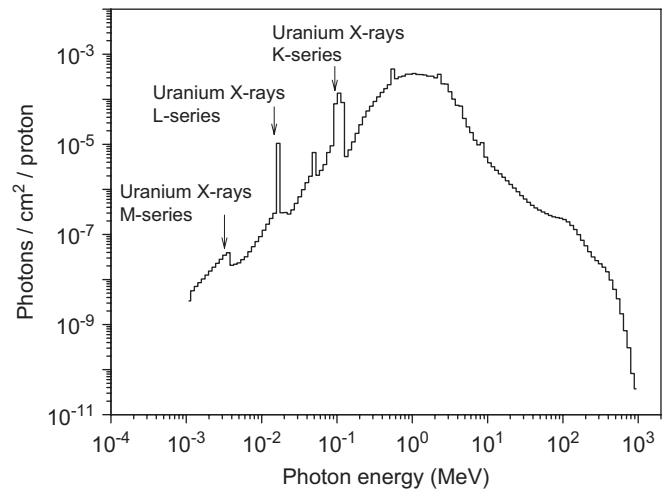


Fig. 9. Average photon flux in the blanket of the EPT setup.

be seen the uranium X-ray peaks appear at their correct energies and spectrum extends to ~ 1 GeV. It should be noted that in MCNPX calculations the correct photon spectrum will be obtained only when all elementary particles whose production (and subsequent decay) is possible at the incident particle energy, are present in the “mode” card and are transported.

In order to estimate the photofission rates, the photon spectra in the MC-FFs were obtained and photofission rates were calculated using the photofission cross-sections given in Refs. [23–27]. Fig. 10 shows the photofission cross-section of ^{238}U as a function of photon energy. In using the

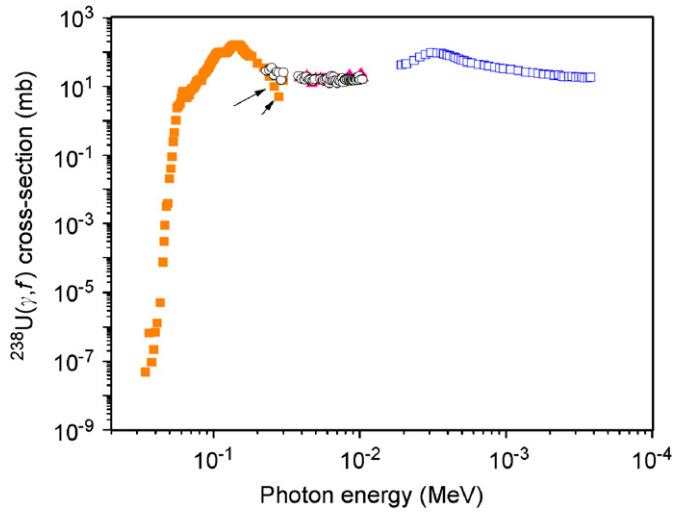


Fig. 10. ^{238}U -photofission cross-section as a function of photon energy. The data were obtained from Refs. [24–28].

cross-section values (Fig. 10) linear interpolation in log–log scale between the data points was used. In Fig. 10 the data points marked with arrows were not used because of their departure from the general trend of the other data point.

The sum of the calculated induced fission rates by neutrons, protons, pions and photons in ^{238}U as well as the experimental results as a function of radial distance for plates at different Z coordinates is shown in Fig. 11.

As it can be seen, by adding the $^{238}\text{U}(p, f)$, $^{238}\text{U}(\pi, f)$ and $^{238}\text{U}(\gamma, f)$ rates to that of the $^{238}\text{U}(n, f)$, the calculated values for the fission rate at $R < 4.2\text{ cm}$ exceed the experimental results on plates at $Z = 0, 11.8$ and 23.6 cm and differences between the experimental and calculations results become less than those shown in Fig. 7 for all data points with $R > 4.2\text{ cm}$ in all sample plates.

The experimental results for R -values beyond the target radius ($R > 4.2\text{ cm}$) for which the accuracy of the track density measurements was 4% were used to determine the deviation of the experiment from the calculation. It was

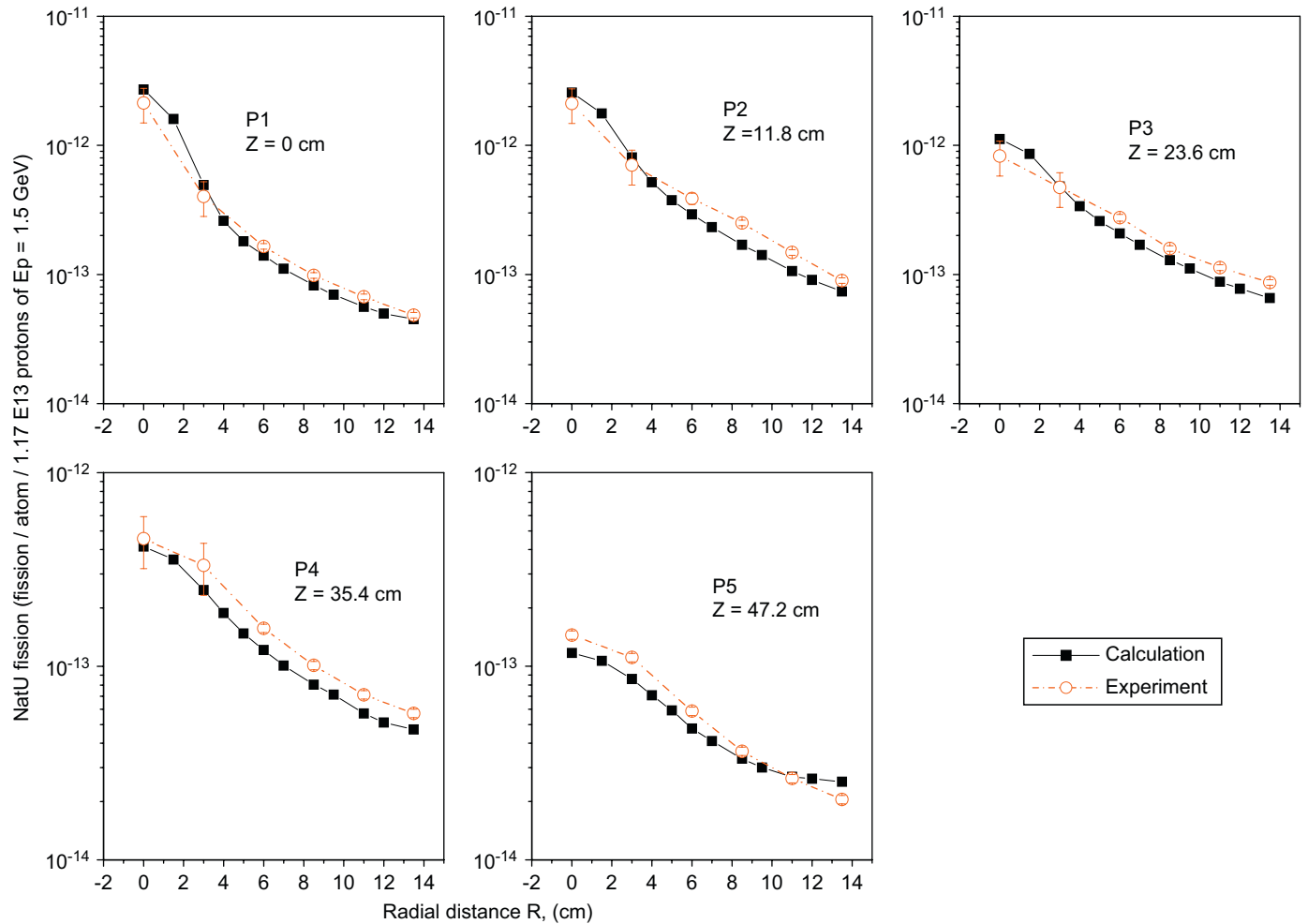


Fig. 11. Variations of the total ^{238}U fission rate (includes the fission induced by neutrons, protons, pions and photons) as a function of radial distance measured from the target axis. The results for five plates at different axial distances, Z are shown. Note that the vertical scale ranges are not the same for all plots and as a result the deviation between the experimental and calculated fission rates are visually suppressed or enhanced. Lines connecting the data points are drawn to guide the eyes.

found that the calculated values are on average less than the experimental results by a factor of 1.22 ± 0.14 .

Further analysis of the results for the *blanket* region suggested that the observed discrepancy between the experimental and calculated fission rates is systematic rather than statistical. This is more evident in the log–log plot of the fission rates as a function of radial distance as shown in Fig. 11. Apart from the data points with $R > 8$ cm in plate 5, the ratio of the experimental results to their corresponding calculated values is almost constant for a given sample plate.

5. Fission-rate distribution along the target axis

Fig. 12 illustrates the variation of the ^{235}U fission rate with distance along target axis for different radial distances. The trends and shapes of the distributions for experimental and calculated results are similar but the magnitudes of the fission rates are different, as discussed earlier.

The MC results of the fission rate as function of Z for each radial distance R can be fitted very well with a third-order polynomial, from which the position of the maximum for each distribution can be calculated. The position of maximum shifts to higher Z -values with increasing distance R .

6. The overall ^{235}U fission rate in the EPT assembly

The MCNPX 2.6C calculations show that in the whole system an interaction of one proton of energy 1.5 GeV with

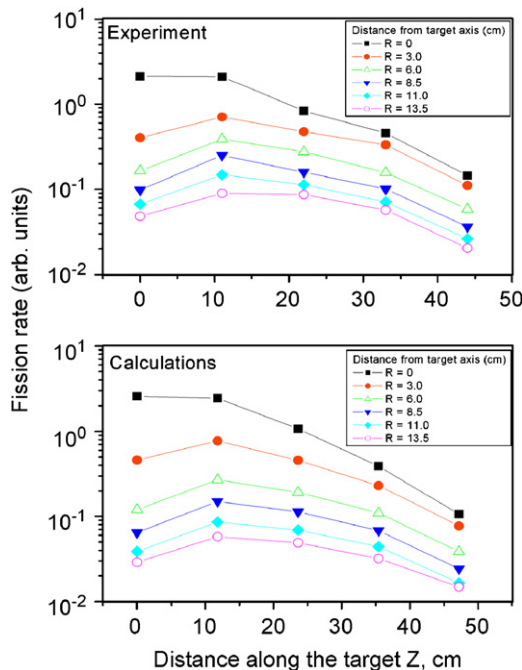


Fig. 12. Total fission rate at different radial distances as a function of distance along the Z -axis for different radial distances, R . Lines connecting the data points are drawn to guide the eyes.

Table 1

Contribution of different fission processes to total number of fission events in the natural uranium blanket

Fission type	Fraction of total number of fissions (%)
$^{235}\text{U}(n, f)$	96.76
$^{235}\text{U}(p, f)$	1.52
$^{235}\text{U}(\gamma, f)$	1.32
$^{235}\text{U}(\pi, f)$	0.40

the target, produces, on average $N_{\text{MC}} = 49.97$ neutrons (escaped neutrons plus captured neutrons), 8.04 protons (including the primary proton), 0.54 pions and 822.3 photons and these result in 5.73 ± 0.15 fissions in the natural uranium blanket. Further calculations showed that contribution of the (γ, xn) reactions to the neutron population in the system is not significant. Table 1 gives the contribution of each of the particles to total number of induced fission events in the *entire blanket*.

An estimate of the total fission rate can be made via fission rate values calculated for the MC-FFs. We used the mean value of the fission rates in all MC-FFs along the $+Y$ and $-Y$ -axes which were beyond the target but were within the blanket area. We obtained mean number of 5.15 ± 0.6 fission per primary proton in the blanket. This value is in agreement with directly calculated value of 5.73 ± 0.15 as discussed above. Such an agreement indicates that if adequate number of fission-foils is distributed within a multiplying medium; the mean fission rate in the system could be obtained from these foils.

We also calculated the number of fission events in the blanket using mean value of the fission rates in the experimental samples in the blanket area. This resulted in total number of (6.29 ± 1.14) fission per incident proton. The large error of 18% in the experimental value of the fission rate in the blanket is the consequence of relatively small number of the samples that were present in the blanket area (15 samples).

7. Possible sources of errors

Most straightforward explanation of the observed discrepancy of 22% is possible if the difference between the experimental and calculated results could be associated with systematic errors in the calibration factor, w and/or the total number of primary protons. However on the basis of the experimental results as given in this paper and those in Ref. [14] we do not believe this is the case. We thus examine all possible sources of the errors in the experiments and MCNPX 2.6C calculations separately.

7.1. Experimental errors

In obtaining the experimental results following sources of error exist.

Table 2

Net neutron yield and number of fission events in the natural uranium blanket of the EPT setup per incident proton of $E_p = 1.5$ GeV

INC physics model	Fission-evaporation model	Net neutron yield (neutrons/proton)	Neutron induced fission per proton		Overall fission per proton, R_{MC}	R_{MC}/R_{exp}
			$E_n \leq 20$ MeV	Total		
BERTINI	RAL	49.97	4.55	5.54	5.73	0.91 ± 0.17
	ORNL	52.66	4.82	5.85	6.04	0.96 ± 0.17
	ABLA	52.92	5.02	6.03	6.23	0.98 ± 0.18
INCL4	RAL	43.75	3.77	4.88	5.04	0.80 ± 0.15
	ORNL	45.61	3.98	5.12	5.29	0.84 ± 0.15
	ABLA	47.07	4.32	5.46	5.65	0.90 ± 0.16
CEM03	–	52.91	4.96	5.94	6.14	0.98 ± 0.18

Calculations were performed using the MCNPX code with different INC physics and fission-evaporation models.

7.1.1. The calibration factor w

Because the track densities in the calibration experiments [14] were in the range of 5×10^4 to 1.0×10^6 tracks cm^{-2} , track density measurements with an error of less than 2% were possible. The other parameters used in determination of the w were the neutron fluence from standard neutron sources with well known fluxes having errors of less than 2% and well known experimentally determined, fission cross-sections for ^{235}U and ^{238}U at energies of thermal and 14.7 MeV. The overall error in w was estimated to be 3%.

7.1.2. Track density measurements

The error in the track density measurements is dependent on the track population in a given sample. For track densities in the range of 10^4 to 3×10^6 the error was 2% at 1σ . In these samples more than 2500 tracks per mica detector were counted. In the samples with track density in the ranges of $(4-7) \times 10^6$ and $(0.8-2) \times 10^7$ the estimated counting error was 30% and 30–50%, respectively. Such high error values for these types of samples result from the fact that in highly populated samples large numbers of tracks overlap and result in underestimation of the track densities. This is responsible for the observed underestimation of the experimental fission rates in the fission-foils at $R < 4.2$ cm in sample plates at $Z = 0, 11.8$ and 23.6 cm as shown in Fig. 11.

7.2. Errors in Monte Carlo calculations

7.2.1. Effects of the intranuclear cascade and fission-evaporation models

In the preceding calculations the Bertini intranuclear cascade and RAL fission-evaporation models have been used. To examine the effects of all other available models we performed the following calculations:

1. Net neutron production in the system (captured + escaped neutrons) was calculated.
2. The fission rate (number of fission events in whole blanket per incident proton) was calculated for two

energy groups of $E_n \leq 20$ MeV and $E_n > 20$ MeV. The cross-section data libraries were same as for earlier calculation. Number of fissions induced by particles other than neutron was calculated using the procedures described in Section 4.2 of this paper.

3. Calculations were performed for INC models of Bertini [11,12], INCL4 [28] and CEM03 [29,30] in combination with RAL [13], ORNL [31] and ABLA [32] fission-evaporation models. It should be mentioned that CEM03 is a self-contained package and fission-evaporation model is built into the code [6,29,30].

Table 2 shows the results. The statistical uncertainties of the calculations were less than 2%. Although within the experimental uncertainties all of the calculated overall fission rates are in agreement with the experimental fission rate in the blanket (i.e. 6.29 ± 1.14), it seems that best agreement is obtained for the case of Bertini+ABLA models and the CEM03 model. The last column of the Table 2 gives the ratio of the calculated values of the fission rate, R_{MC} to the experimental fission rate R_{exp} in the blanket. It was found that if Bertini+ABLA models were used instead of Bertini+RAL models then the deviation between the experimental and calculated fission rates in the foils in the blanket region will be reduced from $22 \pm 0.14\%$ to $13 \pm 0.09\%$.

7.2.2. Effects of the beam centre position

The error in beam centre coordinates (X_c, Y_c) on the target cannot exceed half of the width of the lead–mica sandwich sample placed at the centre of the plate 1 (i.e. 0.35 cm). In order to investigate the effects due to variation in the beam centre coordinates on the calculated fission rates and their spatial distribution, several calculations with different (X_c, Y_c) sets were performed. Fig. 13 illustrates the fission-rate distribution along the Y -axis on plate 5. The vertical axis in Fig. 13 refers to the sum of neutron, proton, pion and photon-induced fissions in the MC-FFs. This figure shows the fission rates for cases in

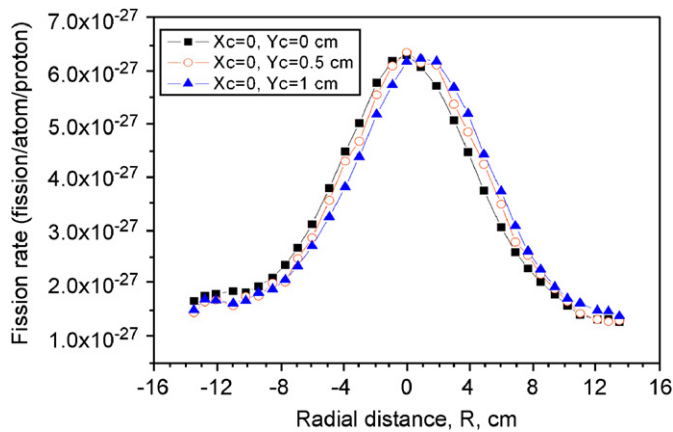


Fig. 13. Total induced fission in U-foils of the plate 5 ($Z=47.2$ cm) for three different beam centre coordinates of (0, 0), (0, 0.5) and (0, 1). Lines connecting the data points are drawn to guide the eyes.

which the beam centre is moved in positive Y -direction (along which the experimental samples were positioned).

Calculations showed that on the average, fission rates in samples along the $+Y$ -axis and in the blanket area increase by 5.5% for $X_c = 0$, $Y_c = 0.5$ cm; 4% for $X_c = 0.5$, $Y_c = 0.5$; and 11.8% for $X_c = 0$, $Y_c = 1$ cm as compared with the case of $X_c = 0$, $Y_c = 0$ cm.

Therefore considering the possible error in the values of the beam centre coordinates (0.35 cm) we conclude that errors on X_c and Y_c cannot introduce more than 5% error in the calculated fission rates.

7.2.3. The beam angle with respect to the target axis

If the target axis was not perfectly parallel with the proton beam axis then this will cause the beam centre to move away from the target axis with different amounts at different Z -positions along the target, regardless of how perfectly the beam centre coincides with target centre at $Z = 0$ cm. Assuming an angle of $0.5\text{--}1^\circ$ between the beam and target axes on plane YZ (Figs. 1a, 2c and 4b), which must have been easily detectable in the course of the experiment setup and beam alignment, the maximum beam centre shift will be 0.41–0.84 cm at the position of the plate 5 ($Z = 47.2$ cm). Calculations showed that such an error on the beam direction cannot cause an average error of more than 5% on the calculated fission rates.

7.2.4. Effects of neutron energy spectrum

Obviously the neutron energy spectrum and its hardness at the position of the MC-FFs and in the blanket as a whole can affect the fission rates. The neutron spectrum within the blanket is determined by (1) the spallation neutron spectrum, (2) the uranium fission neutron spectrum, (3) the spectrum of neutrons from (n, xn) reactions and (4) the material present in the setup and to some extent by the material present in the laboratory environment. In the calculations one can introduce error only via variations in the material compositions and their geometrical arrangements in the code. The Pb target and uranium

blanket were properly built into the code as is evident from Fig. 4. Only some minor approximations were introduced on the geometrical arrangements of the granulated polyethylene shield around the target and on the laboratory environment and its content (cf. Fig. 1a and b with Fig. 4b and a, respectively). Effects of these approximations on the calculated fission rates will be investigated in the following.

To examine the effects of the granulated polyethylene (around the target–blanket assembly) on the ^{235}U fission rate in the blanket the average density of granulated polyethylene (0.7 g cm^{-3}) was altered and the fission rate in the blanket was calculated.

Calculations showed that a variation of the polyethylene density from 0.5 to 0.9 g cm^{-3} (i.e. changing of its mass from 215 to 388 kg) does not change the neutron-induced fission rate in the natural uranium blanket by more than the statistical uncertainties of the calculations which were less than 3%. At the extreme case when all material around the target–blanket was totally removed (see Fig. 5b) the neutron-induced fission rate in the blanket was reduced only by 7.3% presumably due to fission in the ^{235}U component of natural uranium.

In our calculations we added a heavy concrete spherical shell of diameter 8 m and two different thicknesses of 0.5 and 1 m around the EPT setup to take into account the effects of material present in the laboratory and in the walls of the irradiation hall on the neutron spectrum and the calculated fission rates. In both cases this addition did not alter the results noticeably.

8. Conclusions

The fission rate of the ^{235}U in the “Energy plus Transmutation” subcritical experimental setup was measured using fission track technique for incident proton energy of 1.5 GeV. MCNPX-2.6C code was used for transport and simulation of the interactions of the primary and secondary particles in the system.

It is shown that proton-, pion- and photon-induced fissions contribute significantly to the total fission rate in the samples within the target volume and its immediate vicinity. The contribution of protons-, pions- and photon-induced fissions to the overall number of fission events in the blanket does not exceed 1.52%, 0.40% and 1.32%, respectively.

On the basis of the experimental and theoretical results given in this paper, it is evident that in the EPT setup the fission rate of the ^{235}U in the blanket is *not* too sensitive to the modifications introduced to the neutron energy spectrum because of the materials beyond the Cd shielding (Fig. 1). This is due to the fact that, because of the small size and material composition of the target–blanket and samples present in the setup, the neutron energy spectrum is not significantly changed by these modifications. Obviously this will not be the case for isotopes such as ^{235}U for which fission cross-section in the thermal,

epithermal and resonance regions of the neutron spectrum is much higher than that for the ^{235}U .

The beam centre coordinates affect the spatial distribution of the secondary particles in our experimental setup; however, this effect will not be too important when targets with larger diameters are used (especially for positions beyond the target radius), a situation expected to be the case in a realistic ADS.

It is shown that MCNPX 2.6C code prediction of the fission rate is consistently lower by $22 \pm 0.14\%$ than the experimental value for the fission-foils placed in the blanket region, when Bertini and RAL models are used in the calculations. This deviation reduces to $13 \pm 0.09\%$ when the Bertini and ABLA models or CEM03 model are used instead.

From the experimental fission rate measurements, the total number of fission events in the whole blanket was estimated as 6.29 ± 1.14 (fission/proton), which is $22 \pm 0.14\%$ higher than the value calculated using the MC-FFs and (Bertini + RAL) models. Direct calculation of fission rate in the blanket using different INC and fission-evaporation models given in Table 2 showed that best agreement between the experiment and calculation is obtained when Bertini INC model in combination with ABLA fission-evaporation model are used. Also the MC results obtained using CEM03 INC model are in good agreement with the experimental results.

The “Energy plus Transmutation” setup that is used in these experiments provides a unique neutron field which is extended from thermal to relativistic energies. The neutron field in EPT is composed of spallation neutrons with energy spectrum modified to some extent by the EPT environment and fission neutrons. Presence of the polyethylene and Cd shielding around the target–blanket system enhances the number of neutrons at resonance energies (especially on top of the uranium blanket) which is extremely important for nuclear waste transmutation purposes. As a result EPT setup provides an excellent neutron environment for testing the Monte Carlo codes.

The comparison and agreement of the experimental and MC results reported in this paper indicate that the fission track technique along with accurately determined calibration factor provides a correct method for determination of fission rate in a nuclear assembly. Knowledge of fission rate in a multiplying system is essential for determination of effective neutron multiplication coefficient particularly in accelerator-driven systems which are intended to operate in subcritical conditions.

Acknowledgements

We would like to thank Veksler and Baldin Laboratory of High Energies (VBLHE), Joint Institute for Nuclear Research (JINR), Dubna, Russia and staff of the Nuclotron accelerator for providing us the research facilities used in these experiments. Some of us would like to thank JINR for the hospitality during their stay in

Dubna. SRH-N would like to thank the Department of Education, Science and Training of the Government of Australia for the AMRFP grant and the School of Physics, University of Sydney for Denison research grant in support of this work.

References

- [1] C.D. Bowman, E.D. Arthur, P.W. Lisowski, G.P. Lawrence, R.J. Jensen, J.L. Anderson, B. Blind, M. Cappiello, J.W. Davidson, T.R. England, L.N. Engel, R.C. Haight, H.G. Hughes III, J.R. Ireland, R.A. Krakowski, R.J. LaBauve, B.C. Letellier, R.T. Perry, G.J. Russell, K.P. Staudhammer, G. Versamis, W.B. Wilson, Nucl. Instr. and Meth. A 320 (1992) 336.
- [2] C. Rubbia, S. Buono, Y. Kadi, J.A. Rubio, Fast Neutron Incineration in the Energy Amplifier as Alternative to Geological Storage: The Case of Spain, CERN/LHC/97-01, 1997.
- [3] Physics and Safety of Transmutation Systems, A Status Report, OECD 2006, NEA No. 6090, ISBN 92-64-01082-3.
- [4] S.R. Hashemi-Nezhad, R. Brandt, W. Westmeier, V.P. Bablevski, M.I. Krivopustov, B.A. Kulakov, A.N. Sosnin, J.-S. Wan, R. Odoj, Kerntechnik 66 (2001) 47.
- [5] M.B. Chadwick, P.G. Young, S. Chiba, S.C. Frankle, G.M. Hale, H.G. Hughes, A.J. Koning, R.C. Little, R.E. MacFarlane, R.E. Prael, L.S. Waters, Nucl. Sci. Eng. 131 (1999) 293.
- [6] J.S. Hendricks, G.W. McKinney, J.W. Durkee, J.P. Finch, M.L. Fensin, M.R. James, R.C. Johns, D.B. Pelowitz, L.S. Waters, MCNPX, VERSION 26C, Report LA-UR-06-7991, Los Alamos National Laboratory, December 7, 2006.
- [7] M.I. Krivopustov, J. Adam, A. Balabekyan, Y.A. Batusov, M. Bielewicz, R. Brandt, P. Chaloun, D. Chultem, K.K. Dwivedi, A.F. Elishev, M. Fragopoulou, V. Henzl, D. Henzlova, V.G. Kalinnikov, M.K. Kievets, A. Krasa, F. Krizek, A. Kugler, M. Manolopoulou, I.I. Mariin, A. Nourreddine, R. Odoj, A.V. Pavliouk, V.S. Pronskikh, H. Robotham, K. Simon, M. Szuta, V.I. Stegailov, S. Stoulos, A.A. Solnyshkin, A.N. Sosnin, V.M. Tsoupko-Sitnikov, T. Tumendelger, A. Wojecechowski, W. Wagner, J.-S. Wan, W. Westmeier, M. Zamani-Valasiadou, H. Kumavat, H. Kumar, O.S. Zaveriukha, I.V. Zhuk, JINR Preprint E1-2004-79, 2004.
- [8] W. Westmeier, R. Brandt, E.-J. Langrock, H. Robotham, K. Siemon, R. Odoj, I. Adam, V. Bradnova, V.M. Golovatyuk, V.A. Krasnov, M.I. Krivopustov, V.S. Pronskikh, A.N. Sosnin, V.M. Tsoupko-Sitnikov, N.M. Vladimirova, S.R. Hashemi-Nezhad, M. Zamani-Valasiadou, Radiochim. Acta 93 (2005) 65.
- [9] J.-S. Wan, M. Ochs, P. Vater, X.P. Song, E.-J. Langrock, R. Brandt, J. Adam, V.P. Bablevski, B.A. Kulakov, M.I. Krivopustov, A.N. Sosnin, G. Modolo, R. Odoj, Nucl. Instr. and Meth. B 155 (1999) 419.
- [10] A.V. Prokofiev, S.G. Mashnik, A.J. Sierk, Cascade-Exciton Model Analysis of Nucleon-Induced Fission Cross Section of Lead and Bismuth at Energies 45–500 MeV, in: arXiv:nucl-th/9802027 v1, 9 February 1998, LA-UR-98-0418, LANL, Los Alamos, 1998.
- [11] H.W. Bertini, Phys. Rev. 131 (1963) 1801.
- [12] H.W. Bertini, Phys. Rev. 188 (1969) 1711.
- [13] F. Atchison, in: Targets for Neutron Beam Spallation Sources, Jul-Conf-34, Kernforschungsanlage Julich GmbH, January 1980.
- [14] S.R. Hashemi-Nezhad, I. Zhuk, A.S. Potapenko, M.I. Krivopustov, Calibration of track detectors for fission rate determination: an experimental and theoretical study, JINR Report E1-2006-54 (2006) and Nucl. Instr. and Meth. A 568 (2006) 816.
- [15] S.R. Hashemi-Nezhad, I. Zhuk, M. Kievets, M.I. Krivopustov, A.N. Sosnin, W. Westmeier, R. Brandt, JINR Report 2006, in press.
- [16] J.F. Briesmeister (Ed.), MCNP-4B, A General Monte Carlo N-Particle Transport Code, Vol. Report LA-12625, Los Alamos National Laboratory, March 1997.

- [17] P.W. Lisowski, A. Gavron, W.E. Parker, J.L. Ullmann, S.J. Balestrini, A.D. Carlson, O.A. Wasson, N.W. Hill, in: Proceedings of the Specialists' Meeting on Neutron Cross Section Standards for the Energy Region above 20 MeV, OECD/NEA Report NEANDC-305 'U', Uppsala, Sweden, 1991, p. 177.
- [18] P.W. Lisowski, A. Gavron, W.E. Parker, J.L. Ullmann, S.J. Balestrini, A.D. Carlson, O.A. Wasson, N.W. Hill, Proceedings of Nuclear Data for Science and Technology, Springer, Berlin, 1992 (Jülich, Germany, 1991, p. 268).
- [19] R.E. Prael, H. Lichtenstein, User Guide to LCS: The LAHET Code System, Report No. LA-UR-89-3014, Los Alamos National Laboratory, September 1989.
- [20] B. Budick, S.C. Cheng, E.R. Macagno, A.M. Rushton, C.S. Wu, Phys. Rev. Lett. 24 (1970) 604.
- [21] A.V. Prokofiev, Nucl. Instr. and Meth. A 463 (2001) 557.
- [22] H.A. Khan, N.A. Khan, R.J. Peterson, Phys. Rev. C 35 (1987) 645.
- [23] V.V. Varlamov, N.G. Efimkin, V.V. Surgutanov, A.A. Khoronenko, A.P. Chernyaev, in: Fotojad.Dannye-Photofission of U-235, 238 Moscow State University, Nuclear Physics Institute, Moscow (CCP), 1987.
- [24] C. Cetina, P. Heimberg, B.L. Berman, W.J. Briscoe, G. Feldman, L.Y. Murphy, H. Crannell, A. Longhi, D.I. Sober, J.C. Sanabria, G.Ya. Kezerashvili, Phys. Rev. C 65 (2002) 044622.
- [25] H. Ries, U. Kneissl, G. Mank, H. Stroher, W. Wilke, R. Bergere, P. Bourgeois, P. Carlos, J.L. Fallou, P. Garganne, A. Veyssiere, L.S. Cardman, Phys. Lett., Sect. B 139 (1984) 254.
- [26] A. Leprêtre, R. Bergère, P. Bourgeois, P. Carlos, J. Fagot, J.L. Fallou, P. Garganne, A. Veyssière, H. Ries, R. Göbel, U. Kneissl, G. Mank, H. Ströher, W. Wilke, D. Ryckbosch, J. Jury, Nucl. Phys. A 472 (1987) 533.
- [27] J.D.A. Neto, S.B. Herdade, B.S. Bhandari, I.C. Nascimento, Phys. Rev. C 14 (1976) 1499.
- [28] A. Boudard, J. Cugnon, S. Leray, C. Volant, Phys. Rev. C 66 (2002) 044615.
- [29] S.G. Mashnik, A.J. Sierk, Recent Developments of the Cascade-Exciton Model of Nuclear Reactions, Los Alamos National Laboratory Report LA-UR-01-5390, and International Conference on Nuclear Data for Science and Technology, Tsukuba, Japan, October 7–12, 2001.
- [30] S.G. Mashnik, K.K. Gudima, M.I. Baznat, A.J. Sierk, R.E. Prael, N.V. Mokhov, CEM03.S1, CEM03.G1, LAQGSM03.S1, and LAQGSM03.G1 Versions of CEM03.01 and LAQGSM03.01 Event-Generators, Los Alamos National Laboratory Report LA-UR-06-1764, March 6, 2006.
- [31] J. Barish, T.A. Gabriel, F.S. Alsmiller, J.R.G. Alsmiller, HETFIS High-Energy Nucleon-Meson Transport Code with Fission, Oak Ridge National Laboratory Report ORNL-TM-7882, July 1981.
- [32] A.R. Junghans, M.D. Jong, H.-G. Clerc, A.V. Ignatyuk, G.A. Kudyayev, K.-H. Schmidt, Nucl. Phys. A (1998) 635.